



**HAL**  
open science

## Metal-to-ligand charge transfer chirality sensing of d-glucose assisted with GOX-based enzymatic reaction

Junjie Hao, Yiwen Li, Xiaoqian Xu, Fenghuan Zhao, Ruikun Pan, Junzi Li, Haochen Liu, Kai Wang, Jiagen Li, Xi Zhu, et al.

► **To cite this version:**

Junjie Hao, Yiwen Li, Xiaoqian Xu, Fenghuan Zhao, Ruikun Pan, et al.. Metal-to-ligand charge transfer chirality sensing of d-glucose assisted with GOX-based enzymatic reaction. *Advanced Materials Technologies*, 2020, 5 (7), pp.2000138. 10.1002/admt.202000138 . hal-02899871

**HAL Id: hal-02899871**

**<https://hal.science/hal-02899871v1>**

Submitted on 20 Jul 2020

**HAL** is a multi-disciplinary open access archive for the deposit and dissemination of scientific research documents, whether they are published or not. The documents may come from teaching and research institutions in France or abroad, or from public or private research centers.

L'archive ouverte pluridisciplinaire **HAL**, est destinée au dépôt et à la diffusion de documents scientifiques de niveau recherche, publiés ou non, émanant des établissements d'enseignement et de recherche français ou étrangers, des laboratoires publics ou privés.

## **Metal-to-ligand Charge Transfer Chirality Sensing of D-Glucose Assisted with GOX-based Enzymatic Reaction**

*Junjie Hao, Yiwen Li, Xiaoqian Xu, Fenghuan Zhao, Ruikun Pan, Junzi Li, Haochen Liu, Kai Wang, Jiagen Li, Xi Zhu, Marie-Hélène Delville,\* Ming Zhang,\* Tingchao He\* and Jiaji Cheng\**

J. Hao, Dr. Y. Li, R. Pan, Prof. M. Zhang, Prof. J. Cheng  
School of Materials Science and Engineering, School of Computer Science and Information Engineering  
Hubei University  
Wuhan 430062, China  
E-mail: zyybaby@126.com; jiajicheng@hubu.edu.cn

J. Hao, F. Zhao, Prof. M-H Delville  
CNRS  
Univ. Bordeaux  
Bordeaux INP  
ICMCB, UMR 5026  
Pessac, F-33608, France  
E-mail: marie-helene.delville@icmcb.cnrs.fr

Prof. X. Xu  
Department of Developmental Cell Biology, Key Laboratory of Cell Biology, Ministry of Public Health and Key Laboratory of Medical Cell Biology, Ministry of Education, China Medical University, Shenyang, 110122 China

J. Li, Prof. T. He  
College of Physics and Energy  
Shenzhen University  
Shenzhen 518060, China  
E-mail: tche@szu.edu.cn

H. Liu, Prof. K. Wang  
Department of Electrical and Electronic Engineering  
Southern University of Science and Technology  
Shenzhen, 518055, China

J. Li, Prof. X. Zhu  
Shenzhen Institute of Artificial Intelligence and Robotics for Society (AIRS)  
Shenzhen, Guangdong 518172, China

Keywords: chiral sensing, transition metal oxides, metal-ligand charge transfer, D-glucose  
chiral transition metal oxides nanoparticles (NPs) with tunable optical properties are widely accepted as promising toolbox for chiral recognition, stereoselective synthesis and chiroptical devices. Herein, we present chirality-based strategy for discrimination of D-glucose from its

enantiomer through a cooperative synergy between chiral cysteine capped MoO<sub>2</sub> NPs and the glucose oxidase nanosystem. The valence-state-dependent chirality induced by metal-ligand charge transfer (MLCT) effect is found to be ultrasensitive to its redox environment such as the presence of hydrogen peroxide, which is a key indicator of the stereoselective enzymatic reaction between glucose oxidase and D-glucose. With this know-how, glucose enantiomers can be precisely quantified with a limit of detection (LOD) of 0.446 μM. Such a chiral bio-nanosystem would be an ideal platform for a rational design of new types of biosensors, photocatalysts, and chirality based nanodevices.

## 1. Introduction

Recognition of chiral molecules from their enantiomers is of tremendous importance in area of stereoselective synthesis,<sup>[1]</sup> biosensing,<sup>[2]</sup> bio-imaging<sup>[3]</sup> and pharmaceuticals.<sup>[4]</sup> Therefore, developing efficient methods to effectively identify and quantify enantiopure molecules has become a major motivation of modern nanomaterials design. So far, surface-modified metal NPs,<sup>[5]</sup> semiconductors<sup>[6]</sup> and carbon based nanomaterials<sup>[7]</sup> have been well studied for the chiral recognition of biological molecules. However, the current approaches mainly rely on tuning interactions between the surface of nanomaterials and chiral ligands via surface modifications such as chemical bonding and electrostatic attractions.<sup>[2e]</sup> Although great progress has been made, the stability of the nanomaterials and sensitivity for the chiral recognition is still unsatisfied.

Ligand-induced chiral transition metal oxides with tuneable absorption behaviours have attracted great interests because of their widespread potential applications including biosensing,<sup>[8]</sup> hyperspectral imaging,<sup>[9]</sup> and photodetection.<sup>[10]</sup> Kotov and coworkers,<sup>[11]</sup> for instance, reported that chiral WO<sub>3-x</sub> and Co<sub>3</sub>O<sub>4</sub> NPs modified with chiral ligands such as proline, aspartic acid, and cysteine exhibited a strong optical chirality which was even increased by paramagnetism<sup>[11b]</sup> when present. This chirality is induced in their case by

MLCT effects, which are prompted via transitions of the unpaired electrons from the metal- $\delta$  orbitals to the ligand-based  $\pi$  and  $\pi^*$  orbitals indicating that the valence states of the metal atom is of great importance for such an effect. Afterwards, a recent work of ours showed that  $\text{MoO}_{3-x}$  NPs reduced and capped with cysteine could exhibit both plasmonic chirality in the NIR region and strong MLCT chirality in the visible range.<sup>[12]</sup> Although great efforts were made to unveil the underlying origin of the chirogenesis of the MLCT-based chirality, the key parameters, which play a critical role on manipulating such chiral effects and practical applications involving such phenomena, are still to be found. Herein, we present cysteine-modified  $\text{MoO}_2$  NPs, noted as Cys- $\text{MoO}_2$  NPs, with a strong MLCT chirality in the visible range. Based on this MLCT effect, the chiral Cys- $\text{MoO}_2$  NPs are cooperatively combined with glucose oxidase (Gox), a well-known efficient enzyme in terms of chiral recognition of glucose enantiomers as illustrated in **Figure 1**. Since Gox can only catalyze the D-glucose oxidation while remaining inert in the presence of L-glucose,<sup>[13]</sup> the introduction of chiral Cys- $\text{MoO}_2$  NPs can act as an indicator for the sensing of  $\text{H}_2\text{O}_2$  via the MLCT chirality variation. This work fundamentally provides information on the correlation between the MLCT effects / the valence states of the chiral NPs, and their use as a versatile platform for both chiral recognition and quantitative sensing in the area of chiral optics, optoelectronics and biosensing.<sup>[8] [14]</sup>

## 2. Results and discussion

### 2.1. Synthesis and optical characterizations of the chiral Cys- $\text{MoO}_2$ NPs.

The chiral  $\text{MoO}_2$  NPs were synthesized as previously reported in which chiral cysteine molecules were used as both reducing and capping agents.<sup>[12]</sup> The typical TEM image of the as-synthesized L-Cys- $\text{MoO}_2$  NPs in **Figure 2a** shows an average size of  $24.9 \pm 0.8$

nm (Fig. S1 for the size distribution). Strong chiroptical properties were observed in their CD spectrum as shown in **Figure 2b**. Two CD bands at 376 nm and 580 nm, noted as peak (I) and peak (II) hereafter, are recorded respectively showing opposite line shapes depending on the chiral enantiomers of the ligand (note pure L- or D-cysteine has CD bands at 220 nm, **Figure S2**). These results are explained by the link between the chiral cysteine and the MoO<sub>2</sub> core introducing chiral distortions in the NPs lattice and a strong transfer of chirality through the allowed MLCT process, enhanced by the presence of the unpaired electrons in the metal- $\delta$  orbitals. This coupling takes place between these metal- $\delta$  orbitals and the ligand-based  $\pi^*$  orbitals of the cysteine ligand allowing this enhanced chiroptical response in the visible range as illustrated in **Figure S3**. To quantitatively analyse the induced chiral effects, the anisotropic g-factor<sup>[15]</sup> which is defined as  $\Delta\varepsilon/\varepsilon = \Delta A/A$ , where  $\Delta A$  is the absorbance difference between left- and right-handed circularly polarized lights, is calculated for each wavelength as illustrated in **Figure S4**. This g-factor reaches values as high  $6 \times 10^{-3}$  at 376 nm and  $8 \times 10^{-3}$  in the visible range (about 575nm) as compared to the literature.<sup>[11-12]</sup>

X-ray photoelectron spectroscopy (XPS) used to examine the Cys-MoO<sub>2</sub> NPs confirms the valence states of the metal ions. **Figure 2c** shows a typical general survey of D-Cys-MoO<sub>2</sub> NPs with the signal of carbon which is always more or less present because of unavoidable natural contamination, sulphur and nitrogen attesting the existence of cysteine as well as the signal of molybdenum and oxygen. In **Figure 2d**, the fit of the high-resolution XPS spectrum of Mo 3d of Cys-MoO<sub>2</sub> NPs is performed with a splitting energy of  $\sim 3.15$  eV for the Mo 3d<sub>5/2</sub>-Mo 3d<sub>3/2</sub> doublet, and a fixed area ratio of 3:2. The fit requires the use of two positions for the 3d<sub>5/2</sub> peaks of molybdenum, one for Mo(IV) and one for Mo(VI) at 229.2 and 232.5 eV, respectively which are in good agreement with earlier reports.<sup>[16]</sup> The small contribution ( $< 5\%$ ) of this higher oxidation state of

Mo ( $\text{Mo}^{\text{VI}}$ ) may be due to a partial surface oxidation of  $\text{MoO}_2$  nanoparticles.<sup>[17]</sup> The  $\text{Mo}(\text{IV})$  ratio based on XPS results is evaluated to be about 94.8%. The shoulder at 226.9 eV is likely due to the S 2s contribution of cysteine ligand<sup>[18]</sup> grafted on the NP, which can also be confirmed by the S 2p peak at 161.8 eV.

## 2.2. Chiroptical sensing of hydrogen peroxide *via* Cys- $\text{MoO}_2$ NPs.

The chiroptical sensing of hydrogen peroxide was performed with both L and D Cys- $\text{MoO}_2$  NPs, when data for one enantiomer are shown in the main text they are illustrated in the SI for the other one. Since the synthesis of Cys- $\text{MoO}_2$  involves a process in which  $\text{Mo}^{\text{VI}}$  is reduced to  $\text{Mo}^{\text{IV}}$ , it is therefore obvious that oxidation agents could be used to oxidize  $\text{MoO}_2$  ( $\text{Mo}(\text{IV})$ ) into higher valence states with different optical properties. From our previous works,<sup>[12, 19]</sup> we noticed that three main states can be envisioned in which Molybdenum is more or less reduced, such as blue  $\text{MoO}_{3-x}$  NPs with a high valence state close to  $\text{Mo}^{\text{VI}}$ , green  $\text{MoO}_{3-x}$  NPs with a moderate valence state and yellow-brownish  $\text{MoO}_2$  in which molybdenum is mainly  $\text{Mo}^{\text{IV}}$ . Since the presence of unpaired d electrons in the Mo d orbital is the prerequisite for MLCT effects, the existence of  $\text{Mo}^{\text{IV}}$  is critical to preserve the Mo-ligand charge transitions and induce the targeted chirality (**Figure S3**). As a consequence, as soon as  $\text{H}_2\text{O}_2$  is mixed with yellow  $\text{MoO}_2$ ,  $\text{Mo}^{\text{IV}}$  is gradually oxidized into  $\text{Mo}^{\text{VI}}$  and this inevitably negatively influences the MLCT chirality as shown in **Figure 3a** where an increase of  $\text{H}_2\text{O}_2$  induces a decrease of the CD intensity of the MLCT bands no matter the L- or D- Cys- $\text{MoO}_2$  systems indicating that both chiral inorganic NPs were oxidized by the  $\text{H}_2\text{O}_2$  solution. If a large amount of  $\text{H}_2\text{O}_2$  is used, the MLCT bands of both peaks (I) and (II) disappear (**Figure S5**) and the overall solution changes from yellow to blue colour (**Figure S6**) or even colourless (see inserted image in **Figure 3a**) indicating that the majority of the NPs are blue  $\text{MoO}_{3-x}$  with a high valence state of Mo or even a totally oxidized  $\text{Mo}^{\text{VI}}$  as  $\text{MoO}_3$ .<sup>[12]</sup> The corresponding UV-vis.

spectra show a concomitant decrease of the absorption properties of Cys-MoO<sub>2</sub> with the addition of H<sub>2</sub>O<sub>2</sub> as illustrated in **Figure 3b** in the case of L-Cys-MoO<sub>2</sub>. This concomitant and proportional decrease of both the CD signal and UV-vis. intensities does not induce any change in the variation of the calculated g-factor curves ( $g$  as  $\Delta\varepsilon/\varepsilon = \Delta A/A$ ) as illustrated in **Figure 3c**; this parameter is then not relevant to detect H<sub>2</sub>O<sub>2</sub> and we shall focus on the CD variation (**Figure 3d**). Indeed, to quantitatively follow the sensing of H<sub>2</sub>O<sub>2</sub>, the peak (I) CD values vs. the amount of H<sub>2</sub>O<sub>2</sub> are plotted in **Figure 3d**. Apparently, the fitted line shape of both L/D-Cys-MoO<sub>2</sub> systems shows a linear relationship between the CD peak (I) values and H<sub>2</sub>O<sub>2</sub> concentrations over the 0-1 mM concentration range.

In addition, the XPS analysis was applied to monitor the valence states variation after the addition of H<sub>2</sub>O<sub>2</sub>. **Figure S7**, for instance, shows a typical XPS high-resolution spectrum of L-Cys-MoO<sub>2</sub> NPs after reaction with 10 mM H<sub>2</sub>O<sub>2</sub>. The overall spectrum can be fitted considering three types of Mo 3d, doublets: one doublet at 228.8 and 232.0 eV, with a peak energy separation of 3.15 eV assigned to the Mo<sup>IV</sup> 3d<sub>5/2</sub> and Mo<sup>IV</sup> 3d<sub>3/2</sub> of MoO<sub>2</sub>, respectively. Two others, one located at 231.0 eV and 234.2 eV and one at 232.5 eV and 235.7 eV respect are characteristics of MoO<sub>3-x</sub> (Mo<sup>V</sup>) and MoO<sub>3</sub> (Mo<sup>VI</sup>), indicating the surface oxidation of MoO<sub>2</sub> when exposed to H<sub>2</sub>O<sub>2</sub>. As the concentration of H<sub>2</sub>O<sub>2</sub> increases from 0 to 10 mM, the percentage of surface Mo<sup>IV</sup> compared to the overall surface Mo atoms is witnessed to decrease from 94.8% to 48.7% (compare **Figure 2d** and **Figure S7**), as expected from oxidation and in line with the CD measurements as shown in **Figure 3a**. These results confirm the relationship between valence states of Cys-MoO<sub>2</sub> NPs and MLCT chirality, which is highly sensitive to the amount of H<sub>2</sub>O<sub>2</sub>.

### 2.3. Chiral recognition and sensing of glucose enantiomers via Cys-MoO<sub>2</sub>/Gox nanosystem.

With the foregoing know-how that Cys-MoO<sub>2</sub> systems can be utilized for H<sub>2</sub>O<sub>2</sub> sensing with high sensitivity, we are spontaneously motivated to exploit such a capability in applications such as chiral recognition of glucose enantiomers. Since D-glucose is involved in many biological processes and serves as the critical energy source for cells,<sup>[20]</sup> it is therefore of great importance to identify and separate this substance from its enantiomer (L-glucose). As illustrated in **Figure 1**, glucose oxidase (Gox), the well-known biological enzyme, when used to selectively catalyze D-glucose in D-glucono- $\delta$ -lactone produces H<sub>2</sub>O<sub>2</sub> as a by-product while remaining silent in the presence of L-glucose. Hence, when the chiral Cys-MoO<sub>2</sub> systems with ultrasensitive sensing of H<sub>2</sub>O<sub>2</sub> are added as sensors, they are involved as a cooperative sensor of the presence of D-glucose and the detection of its catalytic reaction with Gox.

To illustrate this, we compared the CD spectra of Cys-MoO<sub>2</sub> in the presence of both L-glucose (**Figure 4a-b, Figure S8a**) and D-glucose (**Figure 4c-d, Fig. S8b**) performed separately. L-glucose proved to be inefficient to modify the CD response of the NPs which remained unchanged as shown in **Figure 4a** (pure L/D-glucose only have CD active bands lower than 250 nm, **Figure S9**). Since Gox is silent in the presence of L-glucose, the MLCT based absorptions and corresponding anisotropy g-factor of the systems are not modified (**Figure 4b, Figure S8a**). On the other hand, the use of D-glucose as the reactant induced a decrease of both the CD and UV-vis signals with the increasing concentration of D-glucose (**Figure 4c-d**). Indeed, the latter is oxidized by Gox with the production of H<sub>2</sub>O<sub>2</sub> which is itself immediately detected by the chiral L/D-Cys-MoO<sub>2</sub> NPs. **Figure S8b** shows the corresponding g-factor curves using L/D-Cys-MoO<sub>2</sub> NPs for the reactions. Similar to **Figure 3c**, there is a concomitant decrease of the CD signal and of the optical density linked to the disappearance of L/D-Cys-MoO<sub>2</sub>. This does not modify the anisotropy g of the chiral systems, which remains nearly the same especially at peak (I) position (**Figure S8b**) indicating that the oxidation of Mo(IV) does

affect the MLCT based absorption, but has no impact on the concentration independent g-factor values during the enzymatic reaction.

These results show again that MLCT based absorptions are of critical significance for the induced chirality in Cys-MoO<sub>2</sub> systems and they are closely related to the valence states of the semiconducting core. Additionally, the quantitative evaluation of peak (I) CD values vs. the amount of L-/D-glucose as well as the chiral recognition capability of Cys-MoO<sub>2</sub>/Gox systems are summarized in **Figure 4e** and **Figure S8c-d**. The fitting curves (**Figure 4e**) and summarized performance for detection of glucose (**Figure S8c-d**) show that the Cys-MoO<sub>2</sub>/Gox systems are capable of a precise discrimination between the two glucose enantiomers and a quantitative sensing of D-glucose via a MLCT chirality process with a LOD as low as 0.446 μM for D-Cys-MoO<sub>2</sub>/Gox system (the corresponding CD spectra with 0-50 μM of D-glucose and fitted line for LOD calculations are shown in **Figure S10**). To evaluate the performance of this sensor, it is compared to a list of the analytical performances of already reported assays for the detection of glucose, which is given in **Table 1**; obviously, the obtained LOD of the herein proposed sensing system is lower than the majority of the reported methods, demonstrating the great merits of the proposed method. To avoid the impacts from other sugars in CD performance, various sugar molecules were applied to the enzymatic reaction with the Cys-MoO<sub>2</sub>/Gox system. The corresponding CD measurements in **Figure 5a-b** show that except for D-glucose, all the other sugars including fructose, maltose, xylose, lactose, sucrose and L-glucose are inert to MLCT chirality in terms of CD intensity. The same trend is also observed in the corresponding CD and UV-vis measurements with various amounts of the different sugars (**Figure S11-S12**), proving that the chiral Cys-MoO<sub>2</sub>/Gox systems exhibit a high selectivity only for the glucose without any interference from other sugars.

### 3. Conclusion

In summary, this work establishes a novel chiral sensing toolbox consisting of Cys-MoO<sub>2</sub> NPs triggered by a stereo-selective enzymatic reaction. The intermediate product H<sub>2</sub>O<sub>2</sub> plays as a key role as the indicator for the chiral discrimination and quantitative sensing of the glucose enantiomers. The presence of Mo<sup>IV</sup> in the NPs (with unpaired electrons in the 4d orbital of Mo) is critical to preserve the MLCT transitions and induce the chirality. Different from traditional colorimetric and fluorescence based methods, this technique is based on the CD variation of a sensing system and provides a facile alternative with a high selectivity and sensitivity. It not only offers incisive understanding on MLCT-based chirality of transition metal oxides based chiral systems, but also envisages new insights for chiral recognition and sensing in area of biomedicine, stereo-selective synthesis and biosensing.

#### 4. Experimental Section

*Materials and reagents:* Hydrogen peroxide (H<sub>2</sub>O<sub>2</sub>, 30%), Glucose oxidase (Gox, 100 U/mg), L-(-)-Glucose (98%), D-(+)-Glucose (≥99.5%), D-Fructose (99%), D-(+)-Maltose monohydrate (≥98.0%), D-(+)-Xylose (98%), Lactose (AR,98%), and Sucrose (AR) were purchased from Aladdin (Shanghai, China). Molybdenum disulfide powder (MoS<sub>2</sub>, 99%), L-cysteine (99%) and D-cysteine (98%) were supplied by Macklin (Shanghai, China). All solutions were prepared with deionized water by Wahaha (Hangzhou, China).

*Preparation of aqueous MoO<sub>3</sub> nanoparticles:* The synthesis of MoO<sub>3</sub> NPs follows a previously published method.<sup>[12]</sup> Typically, 0.8 g of pristine black MoS<sub>2</sub> powder (5 mmol) was dissolved in 462.5 mL DI water with vigorous stirring. After that, 37.5 mL 30 wt% H<sub>2</sub>O<sub>2</sub> were added into the as-prepared solution. Then, the black mixture becomes transparent yellow, the overall solution was heated up to 80 °C to remove the excess

H<sub>2</sub>O<sub>2</sub>. After the mixed dispersion becomes transparent and the heat treatment can be stopped.

*Reduction of MoO<sub>3</sub> solution for the synthesis of Cys-MoO<sub>2</sub> NPs:* After obtaining the as-prepared MoO<sub>3</sub> solution (10 mmol/L), the MoO<sub>3</sub> NPs were then reduced and capped via using chiral cysteine molecules following a previously published method.<sup>[12]</sup> Typically, 60 mg of L-cysteine were added into 1.5 mL (10 mM) of the previous as-prepared MoO<sub>3</sub> solution to obtain L-Cys-MoO<sub>2</sub> NPs. Afterwards, the mixture was sonicated for 5 min and incubated in the dark for one week. The same method was applied for D-cysteine to obtain D-cysteine capped MoO<sub>2</sub> nanocrystals. To ensure that the obtained Cys-MoO<sub>2</sub> NPs were well-dispersed in solution, the samples in water solution were all purified via centrifugation 3 min. at 8000 rpm to remove precipitates (if any) and kept at 20 °C before any use.

*Chiroptical sensing of hydrogen peroxide:* In a typical procedure, chiroptical sensing systems with a total volume of 2 ml water solution were pre-prepared, including 200 μL of a 10 mM Cys-MoO<sub>2</sub> NPs (H<sub>2</sub>O) and different amounts of H<sub>2</sub>O<sub>2</sub>. The reaction system was continuously stirred for 30 min. in a ROLLER Shaker. To investigate the response of the Cys-MoO<sub>2</sub> NPs to the H<sub>2</sub>O<sub>2</sub> concentration, different concentrations of H<sub>2</sub>O<sub>2</sub> (200 μM, 400 μM, 600 μM, 800 μM, 1000 μM, 10 mM and 100 mM) were added to the mixture solutions under the same conditions.

*Chiral recognition and sensing of glucose enantiomers using the glucose oxidase (Gox) catalytic reaction:* Firstly, 0.5 ml of Gox and glucose mixture solution was prepared, containing 80 μL of Gox (5 U/μL) and freshly prepared D- or L-glucose solutions at different concentrations. The enzymatic reaction systems were allowed to incubate for 30 min. Then, 1.5 ml of Cys-MoO<sub>2</sub> solution (400 μL, 10 mM) were added to the above solution. The reaction system was continuously stirred for 30 min. on a ROLLER

Shaker. To investigate the response of the Cys-MoO<sub>2</sub> NPs to the glucose concentration, different concentrations of glucose (200 μM, 400 μM, 600 μM, 800 μM, and 1000 μM) were added to the mixture solutions under the same conditions. As for the LOD test, different concentrations of D-glucose (0 μM, 1 μM, 3 μM, 5 μM, 10 μM, 30 μM and 50 μM) were added.

*Selectivity study of the glucose oxidase (Gox) catalytic reaction system:* To probe the selectivity of such chiral recognition system, various sugars were applied to the enzymatic reaction with L-Cys-MoO<sub>2</sub>/Gox system with a given concentration. We further studied the fructose, maltose, xylose, lactose and sucrose. The reaction system is the same as for glucose except for the change of sugar.

*Structural and Optical Characterization:* The UV/Vis absorption spectrum of each sample was recorded using a TU-1901 double-beam UV/Vis spectrophotometer (Beijing Purkin General Instrument Co. Ltd., China). The XPS measurements were performed on a Thermo Scientific™ K-Alpha™ system with a monochromatized Al Kα source ( $h\nu = 1486.6$  eV) and a 200 μm spot size. The samples were prepared via drop casting on a Silicon substrate and possessed sufficient conductivity to prevent any buildup of charge, as judged from a single C 1s peak, which appeared at a constant binding energy of 284.6 (0.2 eV) in all samples. Before insertion of samples in the analysis chamber, a pressure of  $3 \cdot 10^{-7}$  mbar was always reached in the load lock chamber. The high-resolution spectra were acquired by using a constant pass energy of 40 eV although surveys in the 0–1100 eV range were first obtained at a constant pass energy of 200 eV. High-resolution spectra were fitted using the AVANTAGE® software provided by Thermo Fisher Scientific. CD measurements were conducted on a JASCO J-1500 CD spectrometer. The scan rate was 20 nm/min with a data pitch of 0.1 nm. All CD experiments were carried out in a Milli-Q water with a quartz cuvette (0.1 cm path length from Hellma). All optical measurements

were performed at room temperature under ambient conditions. The TEM pictures were taken using a Tecnai F30 microscope working at 300 kV.

### Supporting Information

Supporting Information is available from the Wiley Online Library or from the author.

### Acknowledgements

Junjie Hao and Yiwen Li contributed equally to this work. The work was supported by Innovation Project (Nature Science) of the Universities of Guangdong Province (2018KTSCX198) and open research fund of Key Laboratory for Organic Electronics, and Information Displays. Funding from Shenzhen Institute of Artificial Intelligence and Robotics for Society (AIRS) is appreciated.

Received: ((will be filled in by the editorial staff))

Revised: ((will be filled in by the editorial staff))

Published online: ((will be filled in by the editorial staff))

### References

- [1] a) E. Shah, H. P. Soni, *RSC Adv.* **2013**, 3, 17453; b) X. Jin, Y. Sang, Y. Shi, Y. Li, X. Zhu, P. Duan, M. Liu, *ACS Nano* **2019**, 13, 2804; c) A. Ben-Moshe, A. O. Govorov, G. Markovich, *Angew. Chem., Int. Ed.* **2013**, 52, 1275.
- [2] a) J. Zhou, J. Duan, X.-E. Zhang, Q. Wang, D. Men, *Nanoscale* **2018**, 10, 18606; b) E. Hendry, T. Carpy, J. Johnston, M. Popland, R. V. Mikhaylovskiy, A. J. Laphorn, S. M. Kelly, L. D. Barron, N. Gadegaard, M. Kadodwala, *Nat. Nanotechnol.* **2010**, 5, 783; c) L. Yiye, Z. Yunlong, W. Hai-Yan, P. Sarah, Z. Yuliang, T. Zhiyong, N. Guangjun, *Angew. Chem., Int. Ed.* **2011**, 50, 5860; d) Y. Xia, Y. Zhou, Z. Tang, *Nanoscale* **2011**, 3, 1374; e) W. Ma, L. Xu, L. Wang, C. Xu, H. Kuang, *Adv. Funct. Mater.* **2019**, 29, 1805512.
- [3] a) M. Sun, A. Qu, C. Hao, X. Wu, L. Xu, C. Xu, H. Kuang, *Adv. Mater* **2018**, 30, 1804241; b) R. Gao, L. Xu, C. Hao, C. Xu, H. Kuang, *Angew. Chem., Int. Ed.* **2019**, 58, 3913.
- [4] a) Y.-T. Tseng, H.-Y. Chang, S. G. Harroun, C.-W. Wu, S.-C. Wei, Z. Yuan, H.-L. Chou, C.-H. Chen, C.-C. Huang, H.-T. Chang, *Anal. Chem.* **2018**, 90, 7283; b) K. Soai, T. Shibata, H. Morioka, K. Choji, *Nature* **1995**, 378, 767; c) X. X. Zhang, J. S. Bradshaw, R. M. Izatt, *Chem. Rev.* **1997**, 97, 3313.
- [5] a) E. Zor, N. Bekar, *Biosens. Bioelectron.* **2017**, 91, 211; b) L. Tao, S. Yingying, S. Hongjie, L. Yi, *Analyst* **2013**, 138, 6558.
- [6] Z. Zhang, J. Zhou, Y. Liu, J. Tang, W. Tang, *Nanoscale* **2015**, 7, 19540.
- [7] N. Suzuki, Y. Wang, P. Elvati, Z. B. Qu, K. Kim, S. Jiang, E. Baumeister, J. Lee, B. Yeom, J. H. Bahng, *ACS Nano* **2016**, 10, 1744.
- [8] W. Ma, L. Xu, A. F. de Moura, X. Wu, H. Kuang, C. Xu, N. A. Kotov, *Chem. Rev.* **2017**, 117, 8041.
- [9] M. Hentschel, M. Schäferling, T. Weiss, N. Liu, H. Giessen, *Nano Lett.* **2012**, 12, 2542.
- [10] G. Konstantatos, E. H. Sargent, *Nat. Nanotechnol.* **2010**, 5, 391.
- [11] a) J. Yeom, U. S. Santos, M. Chekini, M. Cha, A. F. de Moura, N. A. Kotov, *Science* **2018**, 359, 309; b) S. Jiang, M. Chekini, Z. B. Qu, Y. Wang, A. Yeltik, Y. Liu, A. Kotlyar,

- T. Zhang, B. Li, H. V. Demir, *J. Am. Chem. Soc.* **2017**, 139, 13701.
- [12] Y. Li, J. Cheng, J. Li, X. Zhu, T. He, R. Chen, Z. Tang, *Angew. Chem., Int. Ed.* **2018**, 130, 10393.
- [13] A. Haouz, C. Twist, C. Zentz, P. Tauc, B. Alpert, *Eur Biophys J* **1998**, 27, 19.
- [14] a) J. Cheng, E. H. Hill, Y. Zheng, T. He, Y. Liu, *Mater. Chem. Front.* **2018**, 2, 662; b) A. Ben-Moshe, B. M. Maoz, A. O. Govorov, G. Markovich, *Chem. Soc. Rev.* **2013**, 42, 7028.
- [15] N. Berova, B. L. Di, G. Pescitelli, *Cheminform* **2007**, 38, 914.
- [16] a) J. G. Choi, L. T. Thompson, *Appl. Surf. Sci.* **1996**, 93, 143; b) D. O. Scanlon, G. W. Watson, D. J. Payne, G. R. Atkinson, R. G. Egdell, D. S. L. Law, *J. Phys. Chem. C* **2010**, 114, 4636.
- [17] H.-S. Kim, J. B. Cook, S. H. Tolbert, B. Dunn, *J Electrochem. Soc.* **2015**, 162, A5083.
- [18] L. Yang, W. Zhou, D. Hou, K. Zhou, G. Li, Z. Tang, L. Li, S. Chen, *Nanoscale* **2015**, 7, 5203.
- [19] Y. Li, J. Cheng, Y. Liu, P. Liu, Z. Tang, *J. Phys. Chem. C* **2017**, 121, 5208.
- [20] T. D. James, K. R. A. S. Sandanayake, S. Shinkai, *Nature* **1995**, 374, 345.
- [21] J. Zhao, X. Hu, X. Huang, X. Jin, K. Koh, H. Chen, *Colloid. Surface. B* **2019**, 183, 110404.
- [22] W. Li, H. Qi, B. Wang, Q. Wang, S. Wei, X. Zhang, Y. Wang, L. Zhang, X. Cui, *Mikrochimi. Acta* **2018**, 185, 124.
- [23] K. Promsuwan, N. Kachatong, W. Limbut, *Electrochimi. Acta* **2019**, 320, 134621.
- [24] X. Bei, K. Li, F. Lei, J. Lu, L. Zhang, *Electrochimi. Acta* **2017**, 239, 36.
- [25] S. Pengfei, X. Yunsheng, *Anal. Chem.* **2014**, 86, 5323.
- [26] Q. Zhi-Bei, Z. Xinguang, G. Li, L. Renmin, S. Dandan, Y. Dajun, S. Guoyue, *Chem. Commun.* **2013**, 49, 9830.
- [27] J. Xian, Y. Weng, H. Guo, Y. Li, B. Yao, W. Weng, *Spectrochim. Acta A* **2019**, 215, 218.
- [28] H. V. Xu, Y. Zhao, Y. N. Tan, *ACS Appl. Mater. Inter.* **2019**, 11, 27233.

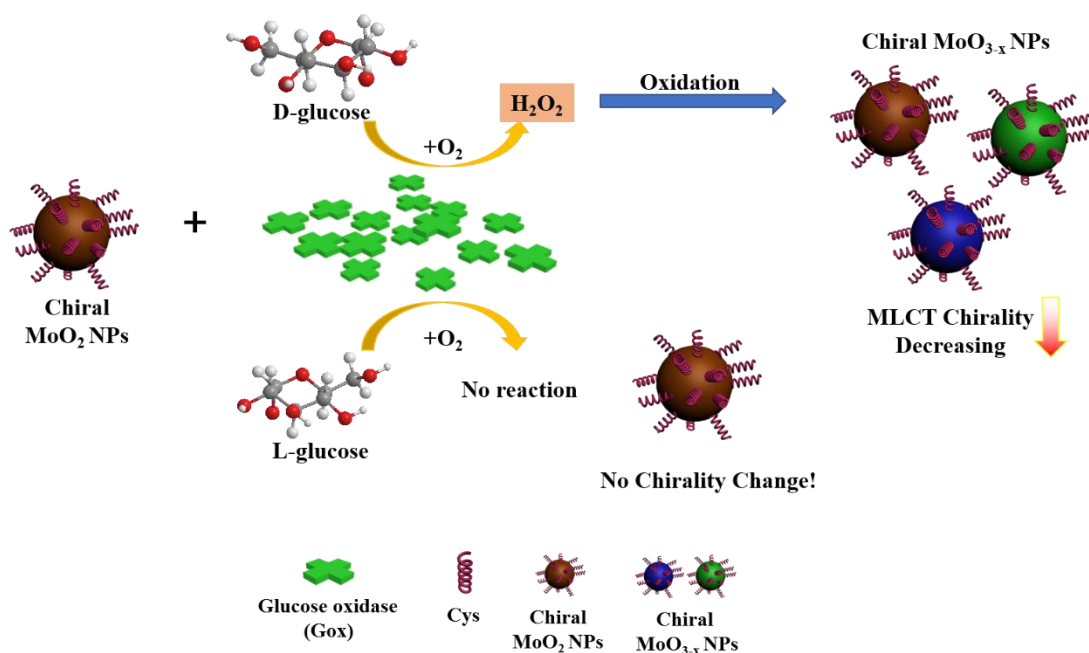


**Figure 1.** A scheme for MLCT chirality-based chiral sensing of the two glucose enantiomers. Glucose oxidase (Gox) selectively oxidizes D-glucose producing  $H_2O_2$  as a by-product, which is detected through the oxidation of  $Mo^{IV}$  to higher valence states and the concomitant decrease of the MLCT chirality in terms of CD performance.

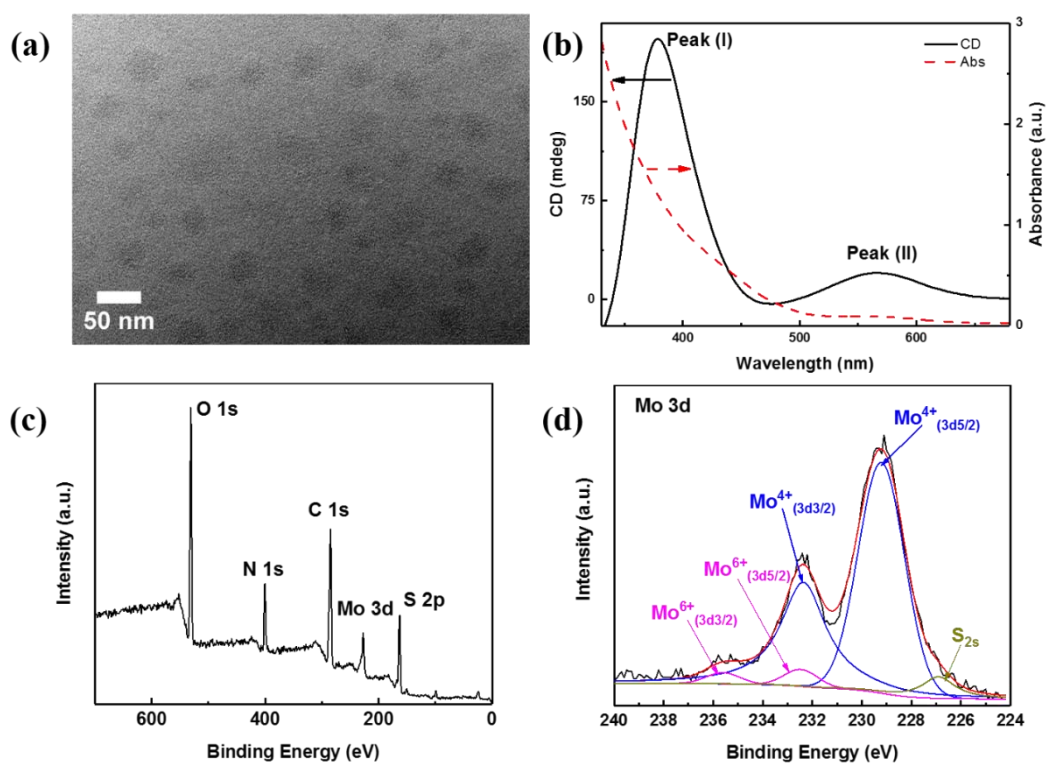


**Figure 2.** Optical characterizations of chiral Cys-MoO<sub>2</sub> NPs. (a) TEM image of D-Cys-MoO<sub>2</sub> NPs; (b) corresponding UV and CD measurements of D-Cys-MoO<sub>2</sub> NPs; (c) XPS general survey; (d) Fit of the high resolution XPS spectrum of the Mo 3d region.

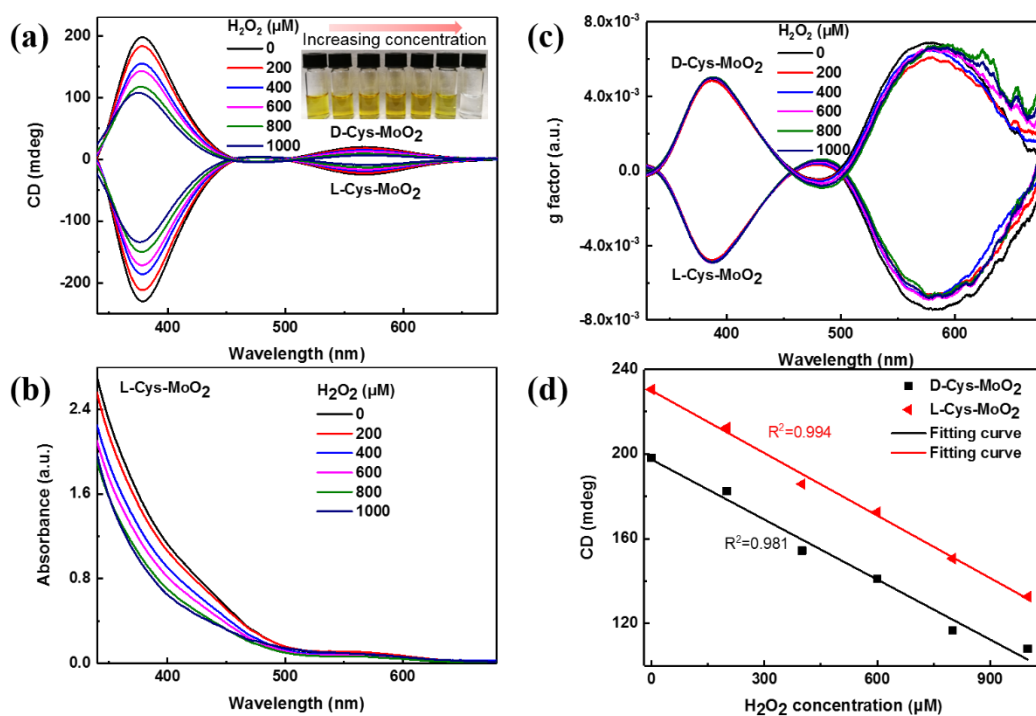


**Figure 3.** Chiroptical sensing of  $\text{H}_2\text{O}_2$  via Cys-MoO<sub>2</sub> NPs chirality follow-up. (a) CD spectra of L-/D- Cys-MoO<sub>2</sub> samples with addition of 0, 200, 400, 600, 800 and 10<sup>3</sup>  $\mu\text{M}$  of  $\text{H}_2\text{O}_2$ . Insert is the image of the solutions after addition of various amounts of  $\text{H}_2\text{O}_2$  as indicated on curves. The very last one (transparent colorless solution) corresponds to a large excess of  $\text{H}_2\text{O}_2$  (> 0.1 M); (b) corresponding UV-vis spectra of L-Cys-MoO<sub>2</sub> samples; (c) corresponding *g*-factor curves of samples in (a); (d) CD peak absolute values at 376 nm vs.  $\text{H}_2\text{O}_2$  amounts and their fitting curves (black line represents the variation for D-Cys-MoO<sub>2</sub> and red line that for L-Cys-MoO<sub>2</sub>).

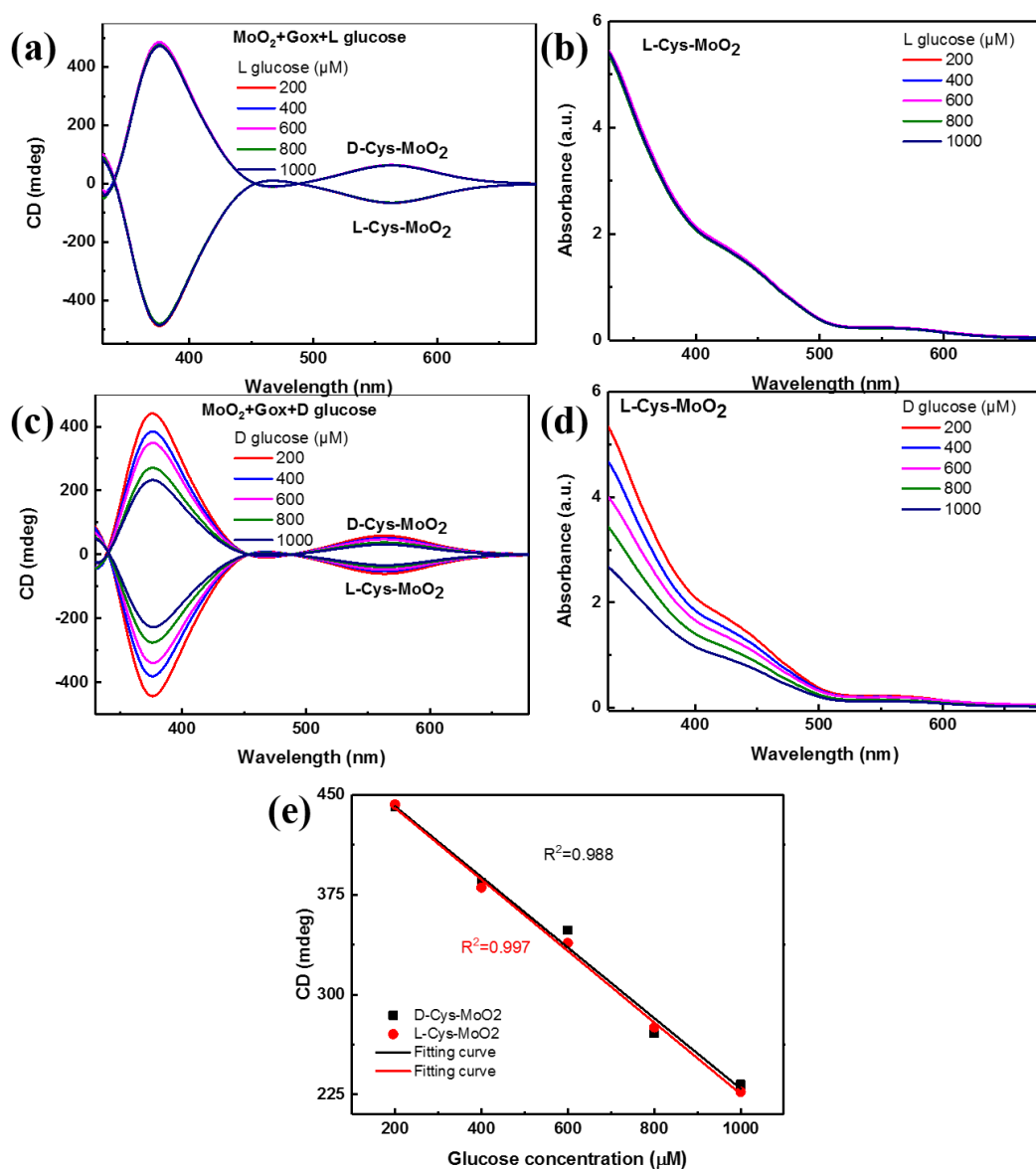


**Figure 4.** Chiral recognition and sensing of glucose enantiomers. (a-b) CD and UV-vis spectra of Cys-MoO<sub>2</sub> involving the enzymatic reaction with different amounts of L-glucose respectively; (c-d) CD and UV-vis spectra of Cys-MoO<sub>2</sub> involving the enzymatic reaction with different amounts of D-glucose respectively; (e) corresponding fitting curves for (c).

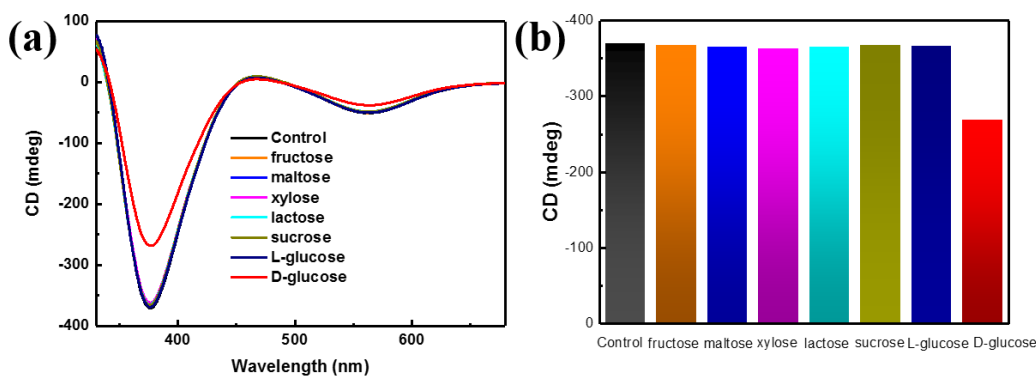


**Figure 5.** Selectivity studies of L-Cys-MoO<sub>2</sub> NPs versus various sugars showing the efficiency as chiral recognition and sensing platform for D-Glucose in the presence of Gox. (a) CD spectra of L-Cys-MoO<sub>2</sub> NPs involved enzymatic reaction with different sugars; (b) a histogram summary of enzymatic reaction with different sugars in terms of CD variation. The concentrations of monosaccharides are 0.6 mM.

**Table 1.** Summary of the analytical performances of reported assays for detection of glucose.

Methods	Sensing system	Line range (μM)	LOD (μM)	Ref
Electrochemistry	D-gel@ AuNPs	0-30000	67	[21]
	NPG <sup>a)</sup> @NiCo <sub>2</sub> O <sub>4</sub>	0-21000	10	[22]
	PdNPs-GNPs <sup>b)</sup> /MWCNTs <sup>c)</sup>	25-10000	8	[23]
	Co <sub>3</sub> O <sub>4</sub> /NiCo <sub>2</sub> O <sub>4</sub> DSNCs <sup>d)</sup> @G <sup>e)</sup>	10-3520	0.384	[24]
Fluorescence	PBA-CDs <sup>f)</sup>	9-900	1.5	[25]
	APBA-GCDs <sup>g)</sup>	100-10000	5	[26]
UV absorption	Fe-CNNPs <sup>h)</sup>	0-100	0.29	[27]
	Ser-Hist Dot @AgNPs <sup>i)</sup>	10-400	53.39	[28]
CD spectra	Cys-MoO <sub>2</sub> /Gox	0-1000	0.446	this work

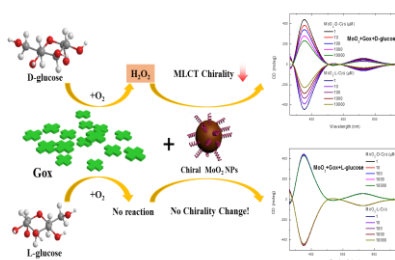
a) NPG: nanoporous gold, b) PdNPs-GNPs: palladium nanoparticle-graphene nanoplatelets; c) MWCNTs: multi-walled carbon nanotubes, d) DSNCs: double-shelled nanocages, e) G: graphene, f) PBA-CDs: phenylboronic acid functionalized carbon dot, g) APBA-GCDs: 3-aminobenzenboronic acid functionalized GQDs, h) Fe-CNNPs: Iron-doped carbon nitride nanoparticles, i) Ser-Hist: serine and histamine biomolecular precursors.

Metal-ligand charge transfer chirality of chiral MoO<sub>2</sub> NPs is found to be sensitive to the redox environment. Such chiral inorganic NPs can cooperatively apply with glucose oxidase for effectively identifying and quantifying glucose enantiomers through valence state variation of molybdenum providing new insights for chiral recognitions and sensing in area of biomedicine.

**Keyword:** chiral sensing, transition metal oxides, metal-ligand charge transfer, D-glucose

Junjie Hao, Yiwen Li, Fenghuan Zhao, Ruikun Pan, Junzi Li, Haochen Liu, Kai Wang, Jiagen Li, Xi Zhu, Marie-Hélène Delville,\* Ming Zhang,\* Tingchao He\* and Jiaji Cheng\*

### Metal-to-ligand Charge Transfer Chirality Sensing of D-Glucose Assisted with GOX-based Enzymatic Reaction



## Supporting Information

### **Metal-to-ligand Charge Transfer Chirality Sensing of D-Glucose Assisted with GOX-based Enzymatic Reaction**

*Junjie Hao, Yiwen Li, Xiaoqian Xu, Fenghuan Zhao, Ruikun Pan, Junzi Li, Haochen Liu, Kai Wang, Jiagen Li, Xi Zhu, Marie-Hélène Delville,\* Ming Zhang,\* Tingchao He\* and Jiaji Cheng\**

J. Hao, Dr. Y. Li, R. Pan, Prof. M. Zhang, Prof. J. Cheng  
School of Materials Science and Engineering, School of Computer Science and Information Engineering  
Hubei University  
Wuhan 430062, China  
E-mail: zyybaby@126.com, jiajicheng@hubu.edu.cn

J. Hao, F. Zhao, Prof. M-H Delville  
CNRS  
Univ. Bordeaux  
Bordeaux INP  
ICMCB, UMR 5026  
Pessac, F-33608, France  
E-mail: marie-helene.delville@icmcb.cnrs.fr

Prof. X. Xu  
Department of Developmental Cell Biology, Key Laboratory of Cell Biology, Ministry of Public Health and Key Laboratory of Medical Cell Biology, Ministry of Education, China Medical University, Shenyang, 110122 China

J. Li, Prof. T. He  
College of Physics and Energy  
Shenzhen University  
Shenzhen 518060, China  
E-mail: tche@szu.edu.cn

H. Liu, Prof. K. Wang  
Department of Electrical and Electronic Engineering  
Southern University of Science and Technology  
Shenzhen, 518055, China

J. Li, Prof. X. Zhu  
Shenzhen Institute of Artificial Intelligence and Robotics for Society (AIRS)  
Shenzhen, Guangdong 518172, China

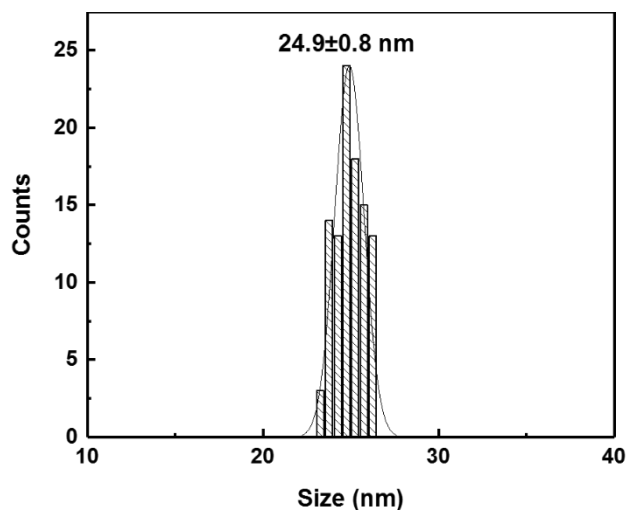


**Figure S1.** Size distribution for D-Cys capped MoO<sub>2</sub> nanoparticles via HRTEM observation based on 100 individual NPs.

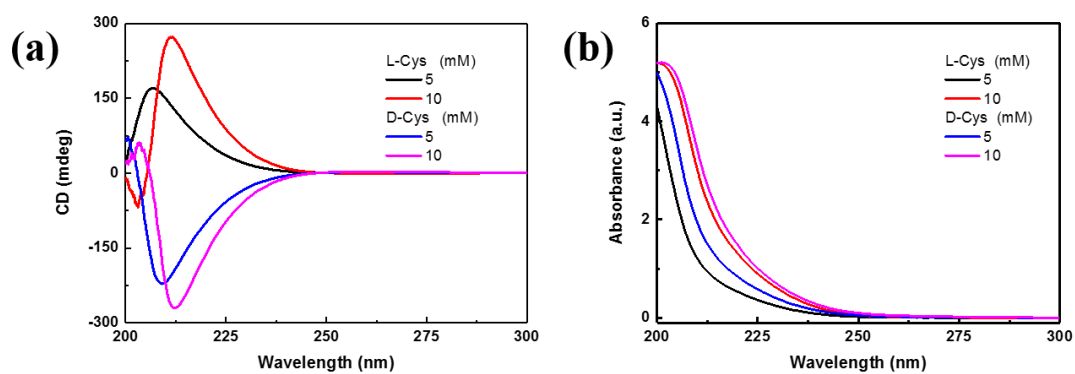


**Figure S2.** CD and corresponding UV-vis measurements of pure L/D cysteine molecules with 5 and 10 mM in concentration.

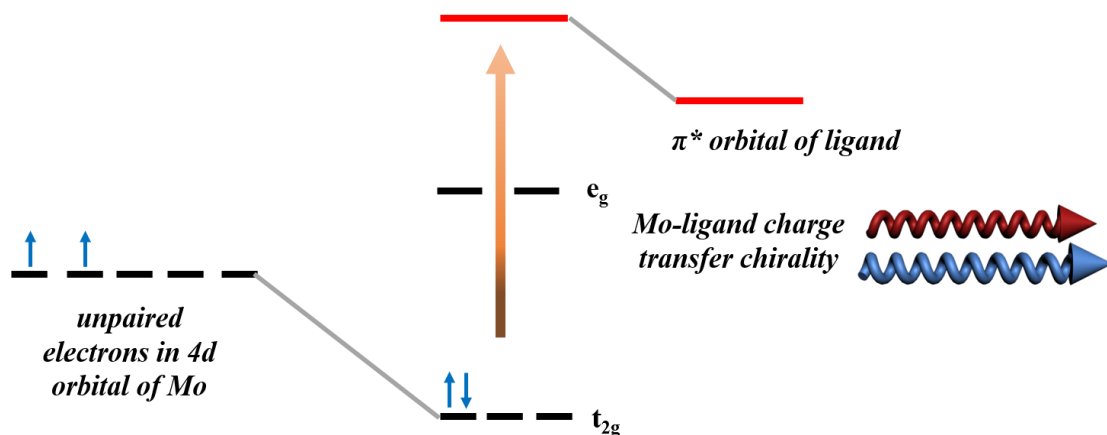


**Figure S3.** Illustration of Metal-Ligand charge transfer chirality for Mo and cysteine molecules.

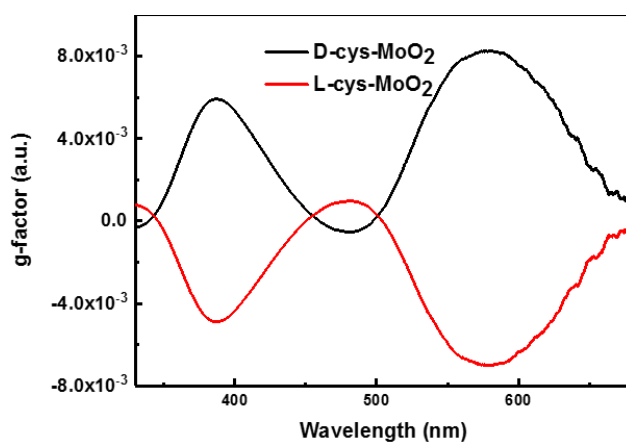


**Figure S4.** *g*-factor curves of as-synthesized pure L-/D-Cys MoO<sub>2</sub> NPs.

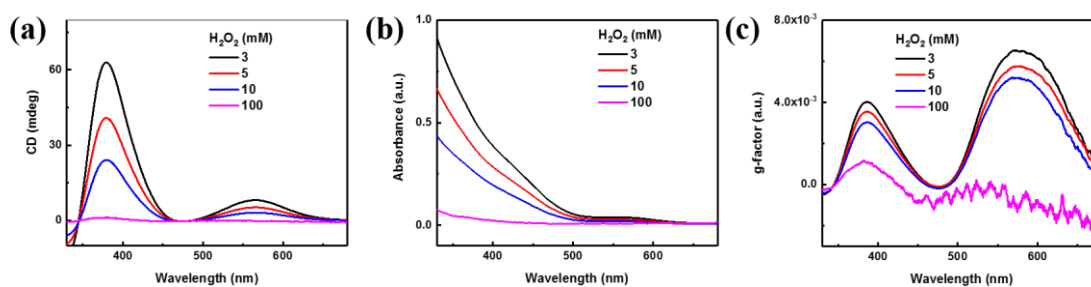


**Figure S5.** Chiroptical sensing of large amounts H<sub>2</sub>O<sub>2</sub> *via* Cys-MoO<sub>2</sub> NPs. (a) CD spectra of D-Cys-MoO<sub>2</sub> samples with addition of concentrations as high as 3, 5, 10, and 100 mM of H<sub>2</sub>O<sub>2</sub>. (b) corresponding UV-vis spectra of D-Cys-MoO<sub>2</sub> samples. (c) corresponding *g*-factor curves of samples in (a).



**Figure S6.** Image of L-Cys-MoO<sub>2</sub> samples with addition of 0, 200, 400, 600, 800, 1000 and 10<sup>4</sup> μM of H<sub>2</sub>O<sub>2</sub>.

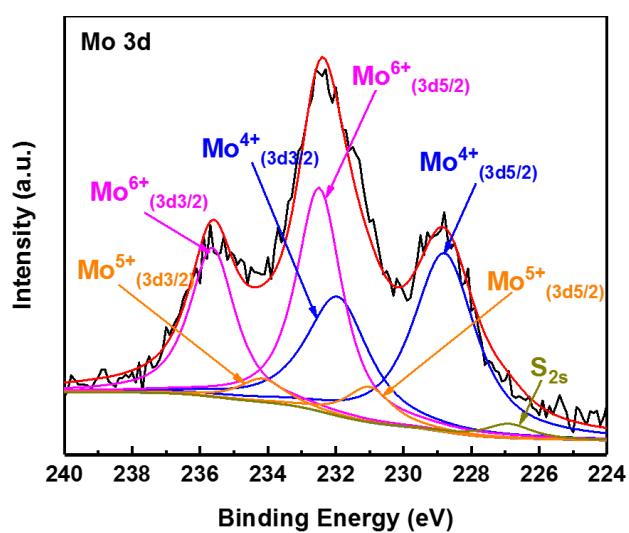


**Figure S7.** Typical XPS high-resolution spectrum of Mo 3d region after addition of 10 mM H<sub>2</sub>O<sub>2</sub> to L-Cys-MoO<sub>2</sub>.

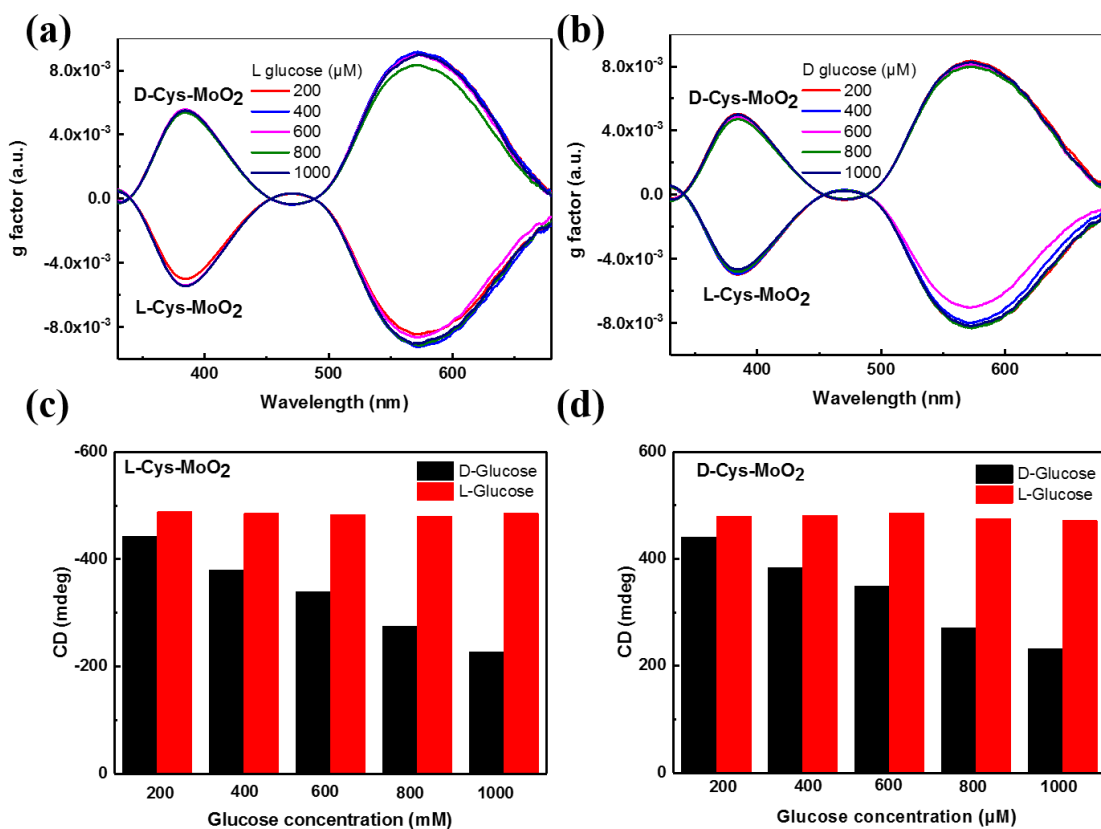


Figure S8. Chiral recognition and sensing of glucose enantiomers corresponding to Figure 4. (a, b)  $g$ -factor curves of Cys-MoO<sub>2</sub> involving the enzymatic reaction with different amounts of L-glucose and D-glucose, respectively; (c, d) summary of chiral recognition and sensing of glucose enantiomers based on L- and D-Cys-MoO<sub>2</sub> NPs.

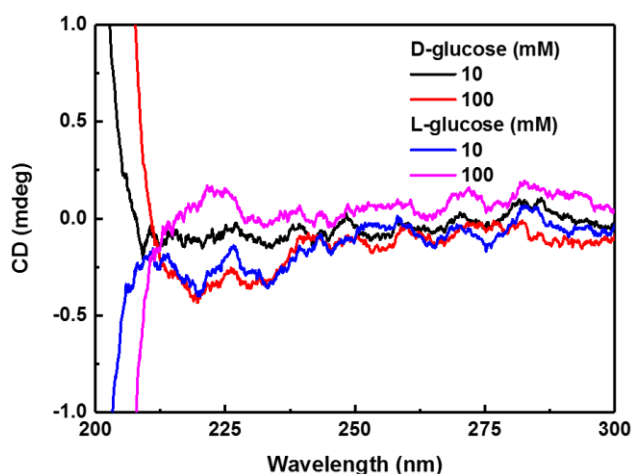
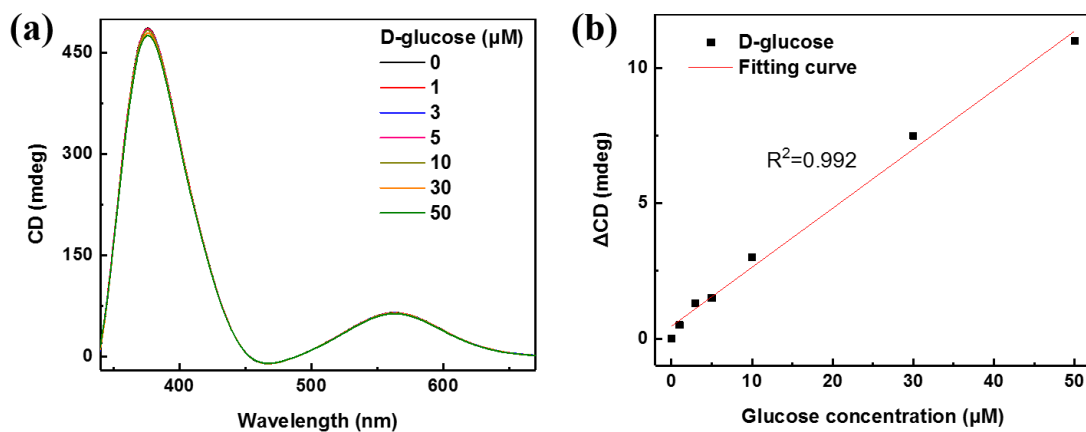
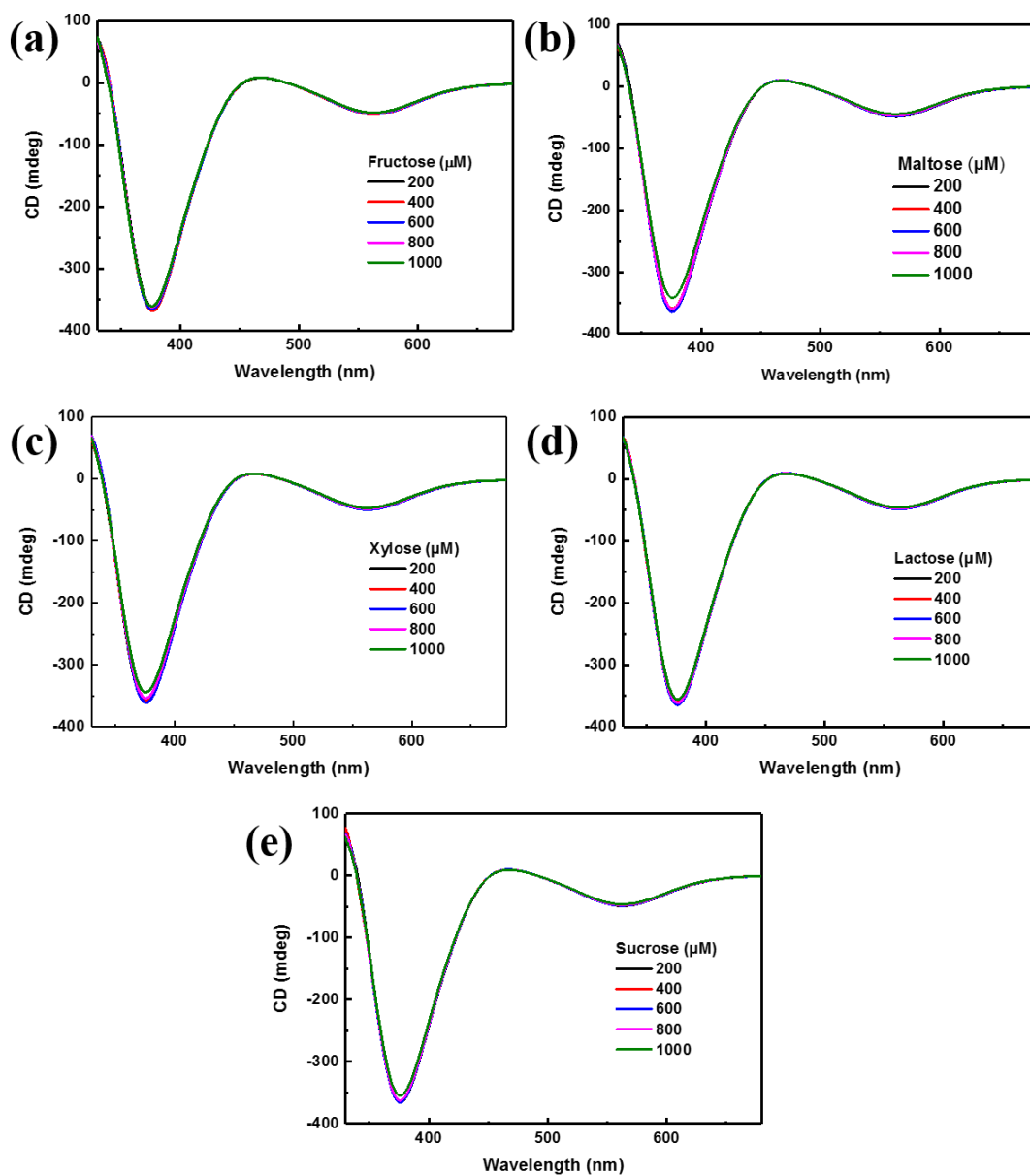


Figure S9. CD measurements of pure L/D glucose molecules with 10 and 100 mM in concentration.



**Figure S10.** (a) Chiral recognition and sensing of D-glucose with D-Cys-MoO<sub>2</sub>/Gox with concentrations of D-glucose from 1  $\mu\text{M}$  to 50  $\mu\text{M}$  and (b) the  $\Delta\text{CD}$  dependence on concentration leading to the LOD value.



**Figure S11.** CD measurements of the L-Cys-MoO<sub>2</sub> in the L-Cys-MoO<sub>2</sub>/Gox based enzymatic catalysis with different concentrations of fructose (a), maltose (b), xylose (c), lactose (d) and sucrose (e).

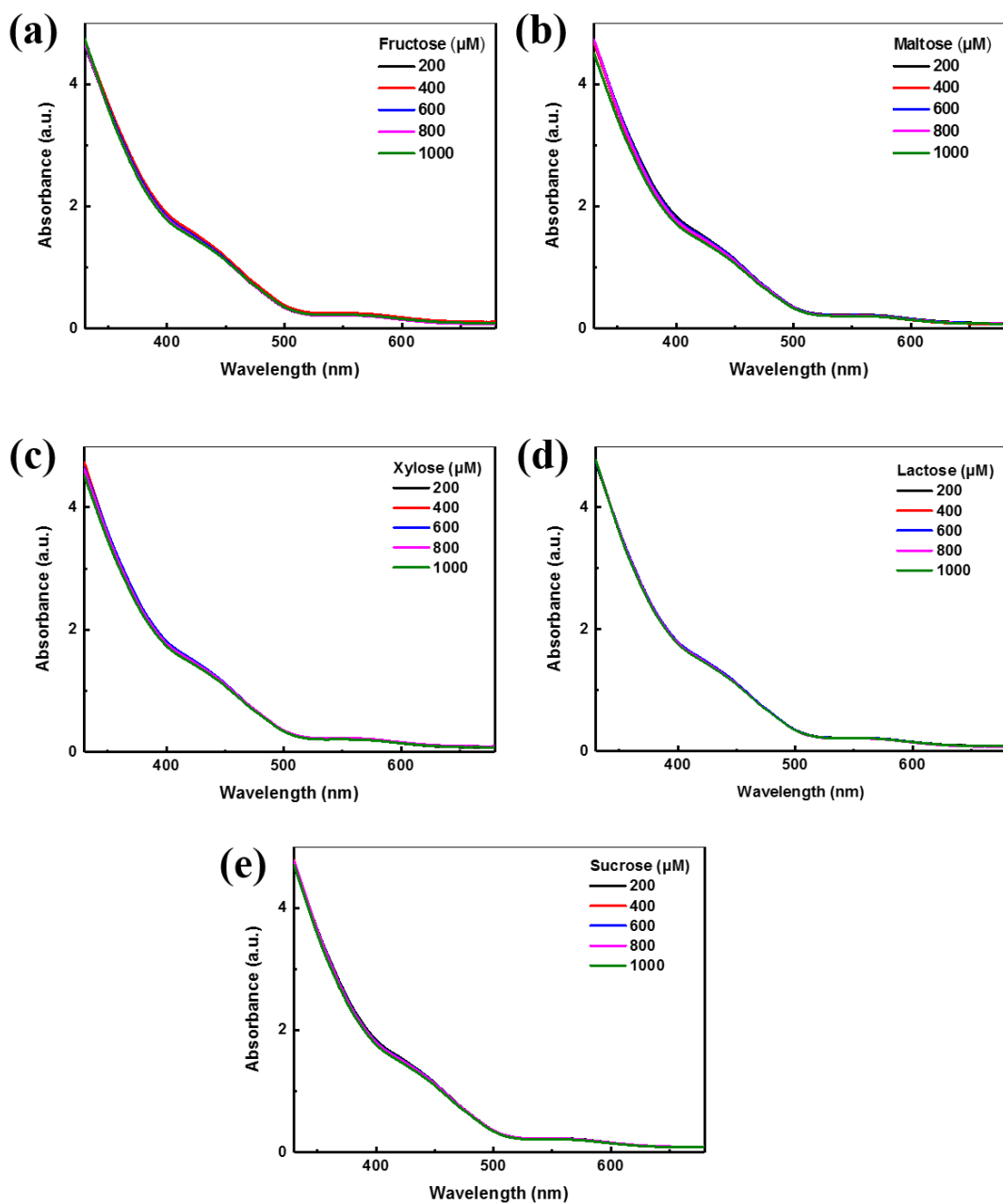


**Figure S12.** UV-vis spectra of the L-Cys-MoO<sub>2</sub> NPs in the L-Cys-MoO<sub>2</sub>/Gox based enzymatic catalysis with different concentrations of fructose (a), maltose (b), xylose (c), lactose (d) and sucrose (e).